Society for Science and Education
United Kingdom

ISSN: 2055 - 1266
Volume 4 No 4
Aug 2017

Journal of Biomedical Engineering and Medical Imaging

TABLE OF CONTENTS

EDITORIAL ADVISORY BOARD	I
DISCLAIMER	II
Hybrid Algorithm Edge Detected DICOM Image Enhancement and Analysis based on Genetic Algorithm for Evolution and Best Fit Value S Chetan, H S Sheshadri andV Lokesha	1
Finger Movement Identification Using EMG Signal on the Forearm N. Sheikh, F. Muhammad, M. F. Shamim, N. Shahid, S. M. Omair, and M. Z. Ul Haque	12
Automated Pulmonary Lung Nodule Detection Using an Optimal Manifold Statistical Based Feature Descriptor and SVM Classifier Ammi Reddy Pulagam, Venkata krıshna Rao Ede, Ramesh Babu Inampudi	20

EDITORIAL ADVISORY BOARD

DISCLAIMER

All the contributions are published in good faith and intentions to promote and encourage research activities around the globe. The contributions are property of their respective authors/owners and the journal is not responsible for any content that hurts someone's views or feelings etc.

SOCIETY FOR SCIENCE AND EDUCATION UNITED KINGDOM

JBEMi JOURNAL OF BIOMEDICAL ENGINEERING AND MEDICAL IMAGING

ISSN: 2055-1266
VOLUME 4 ISSUE 4

Hybrid Algorithm Edge Detected DICOM Image Enhancement and Analysis based on Genetic Algorithm for Evolution and Best Fit Value

[1]S Chetan, [2]H S Sheshadri, [3]V Lokesha

[1] Department of ECE, Dr. Ambedkar Institute of Technology and Research Scholar, Jain University, Bengaluru, India;

[2]Department of ECE, PES College of Engineering, Mandya, India;

[3]Department of Mathematics, Vijayanagara Sri Krishnadevaraya University, Bellary, India;

chetan.s@dr-ait.org;

ABSTRACT

The segmentation of a DICOM standard medical image is a necessary technique which is essential for feature extraction, object edge detection and classification of the segments of the image. The DICOM image is partitioned based on the Hybrid ACO-CPM algorithm, based on the edges in the image, for analysis. The edges are seen as the boundaries within the image which differentiates different regions in the image. The factors that links to the boundary discontinuities that co-exists between the pixels of DICOM image, like texture, intensity and gradient are rendered redundant and are taken care with the application of the Hybrid ACO-CPM algorithm. DICOM image features correspond to that of meta-heuristic characteristics, which are considered during the application of Hybrid ACO-CPM algorithm. The results obtained from this non-deterministic behavior needs to be optimized over a large space called as the search space, wherein the lists of all possible solutions are provided. Each solution is to be marked as a value fit to be termed problematic and needs to be synthesized for an optimized solution. Among various techniques that provide solutions in obtaining an equitable optimization solution, Genetic Algorithms (GA) corroborates as one of the persuasive techniques in a large search space.

In this paper we propose an efficient and effective workflow based on a methodology, that provides an overview of the image enhancement and object classification for a DICOM image using Genetic Algorithm (GA). The edge detected medical standard DICOM image obtained from the Hybrid ACO-CPM algorithm is modified with respect to critical edge data. With the application of GA methodology, the process of enhancing the image ultimately suffices by rendering an image suitable for a specific application with an improved visual quality of the segmented image. A Figure-of-Merit is constructed to differentiate between the image metrics and their best fit values obtained for the images with respect to the Ant Colony Optimization (ACO) algorithm and proposed Hybrid ACO-CPM algorithm, upon enhancing the images using GA

DOI: 10.14738/jbemi.44.3412
Publication Date: 17th August 2017
URL: http://dx.doi.org/10.14738/jbemi. 44.3412

Keywords: DICOM Image, Ant Colony Optimization (ACO), Hybrid Ant Colony Optimization-Critical Path Methodology (ACO-CPM), Genetic Algorithm (GA), Image Enhancement

1 Introduction

The mechanism of natural selection and genetics are based on the principles of selecting and evolving the solution with respect to the global search space, and produce results at each genetic evolution cycle termed as generation. This is one of the most widely accepted and adaptive parallel search techniques that speculate with the potential solutions for the search points correlated within the search space. The Genetic Algorithm (GA) [1, 2, 3] improves the performance of a search algorithm using the genetics that are using the exhilarated operators corresponding to the attributes for the seizure of potential solutions iteratively. GAs tends to provide optimization solution to the stochastic optimization methods over conventional optimization methods without and priori information about the functions of the optimization algorithms. This is performed based on the operators used by the GA such as;

i. Selection
ii. Cross-over
iii. Mutation

An algorithmic model with a providently large population of entities operating in retrieving certain information for a designated analysis purpose is considered as a major concern, wherein the amount of solutions provided will be huge. In image processing, during the image segmentation process based on the information contained within the edge image, suitable optimization algorithms are applied in retrieving the edge information from the image for various analytical purposes. These optimization algorithms, stochastic in nature and continue to adapt to perform with the change in the image environment. The complex behavior of the optimization algorithms, with an undefined population set of operators performing the search operation in finding the edge within the image appeals for sourcing of enormous amount of possibilities of solutions. Such an instance is provided with the application of Ant Colony Optimization (ACO) [6] algorithm, wherein the edge detected by defined set of ant population results in a functional form of image sets, without the prior knowledge of the image statistics. Similarly as with the case of Hybrid Ant Colony Optimization-Critical Path Methodology (ACO-CPM) [5], the pre-defined populations of ants are being segregated as real and virtual ants in optimizing the image edge information retrieval process provides with huge set of solutions, with the information of the Critical Path identified for a particular population set. This has to be improved with the extraction of finer details in the images as obtained from these optimization algorithms.

The DICOM image is a medical standard digital image, used for various telemedicine applications. This kind of an image is exposed to the optimization algorithms in retrieving the information about the edge contained within the image. These edges in the DICOM images contain valuable information about the image, used during object classification for image analysis, for various diagnostic purposed. Hence the resultant quality of the image obtained from the optimization algorithms bearing the necessary information about the image has to be improved with their visual quality attributes. And also it is required to optimize the solution set from the global search space, a space with collection of solutions in detecting the edge of the image. There is zero impact on the image data content with the application of GA. The application of GA and its operators increases the dynamic range of the features contained within the image, thereby improving the visual appearance of the image and also remove the noise from

the image. This process also highlights the objects edge in the selected DICOM image. The process which optimizes the global search by selecting an appropriate image enhancement parameter from the image data, automatically, is also demonstrated in this paper.

2 Elements of Genetic Algorithm and the need for Evolution

Genetic Algorithms are evolutionary computation methodologies [4], which considers the following aspects; population of chromosomes, selection based on fitness value, cross-over for the production of new off-springs, cross-over rate and mutation rate. GA is a kind of search algorithm that computes the single solution considering multiple solutions, from the search space. In Genetic Algorithm (GA), terms like chromosome, mutation, cross-over are clearly defined. The term chromosome in GA refers to an optimal solution that corresponds to a problem defined. This chromosome is considered as a bit string that is encoded. The term gene correspondingly refers to single bits or short blocks of adjacent bits that are used to encode a particular element in a solution as obtained by the processing algorithm. The bits that encode a parameter in the stochastic optimization algorithms are regarded to be genes. Similarly, cross-over means that bit string which is obtained during the exchange of genetic information between the parents information (i.e. the information contained in the file before the application of the GA). Mutation is the basic process of flipping the bit at a randomly chosen locus point with the new bit.

The basic idea behind the application of GA in any domain is to obtain an optimized solution among a set of solutions which is repeated with a factor being common among them. The search space is a context wherein an infinite set of all possible solutions are accumulated. The terms under which the solution set is optimized, an assumption that there shall be a representation within the search space, wherein all the possible genotypes with their fitness values are being considered for sorting. The sorting is done if there happens to be a correlation between the quality of each of the neighboring solutions with the same fitness values are to be sorted and segregated as the optimized solution. Here the fitness values are plotted and can be seen with some evolution. Meaning, the population set tends to move along the pane towards the local peaks, by means of adaptation. The evolution is necessary as the environment in which the population is inhabited with certain fitness values, independent of the other, may be induced with an increase in their population value. This result in the change of the fitness values of the genotypes and the set with the best fit values are to be retained in contention among the other population set. Most often, GAs assigns the fitness scores to the number of chromosomes in the current population based on the fitness function defined. It is also dependent on the GA operators which are of three types;

i. ***Selection:*** This value is set by the operator to decide upon the reproduction factor from the population set. The more fitter is the chromosome; it is likely to reproduce more number of times.

ii. ***Crossover:*** The locus is chosen randomly and the bit strings are exchanged from the latter and former local points from the current locus. This exchange is between the chromosomes from the latter and former local points from the current locus, which results in the generation of two off-springs.

iii. ***Mutation:*** The operator which randomly flips the bits in the string of the chromosome. This is a random process which might happen with a infinitesimally small probabilistic value.

The GA basically provides a methodology with which the highly fit strings with a comparatively fitness values in the search space are searched and identified as the best possible optimized solutions.

3 Literature Survey

The application of the concept of Genetic Algorithm (GA) in image processing problems [7, 8, 9], in order to achieve an optimal solution upon the performance of an efficient and effective search in the complex search space. The image contrast enhancement for an image obtained through gray-level modification with certain image statistics, can be performed as proposed by Sankar K Pal et.al [10], with the application of GA. The important aspects in digital image processing is to enhance the visual quality of the image, much better than that of the original image that can be used for specific applications was proposed by Shivangini et.al [11]. They had considered a gray-scale digital image and its enhancement with the consideration of N-point crossover as improvised against the generic GA. Additional noise from the image was successfully removed and the resulting imaging was restored with originality without any change in the data content of the image. The effect of increasing gray intensity with a dynamic range in the input image was improvised with the proposal of contrast enhancement technology. This technology was based on the Histogram Equalization (HE), called Adaptively Increasing Histogram Equalization (AIVHE). This was successfully demonstrated and proposed by S Palanikumar et.al [12] for Palm-print Enhancement. They used the optimized gamma and beta parameters based on their entropy values, in order to obtain an enhanced palm-print and also maintained the integrity of the data content of the image. Here in this proposal they considered the entropy values as the basis of fitness functions. The soft computing method of GA was proposed and implemented by Komal R Hole et.al [13]. This method was used to enhance the quality of the image and to convert the image into segments to retrieve more meaningful image for analysis using GA.

With an increase in digital imaging in the field of medicine, tumor detection is an important and challenging task that needs to be addressed. Amanpreet Kaur et.al [14] proposed a methodology in reducing the population set of brain tumor images by clustering and genetics, thereby reducing the area of concentration. The genetics are re-implemented for an effective detection of tumor from the concentrated area.

4 Methodology and Workflow

The concept of image enhancement promises with the process of improvising the visual quality attribute of the digital image. The noise from the image is removed and the qualitative features of the image are identified and enhanced with the application of GA. The methodology proposed in the paper considers the edge detected image processed from the Hybrid ACO-CPM algorithm, proposed by Chetan S et.al [5]. The DICOM standard medical image is converted into bitmap format (.bmp) and processed by Hybrid ACO-CPM upon Image Approximation [15]. The processed image from the hybrid algorithm which is also in the bitmap format (.bmp) is considered as an input into the GA. The behavior of the ants in this Hybrid ACO-CPM in detecting the edge of a DICOM image is considered as a combinatorial problem.

Here in this GA for the edge detected DICOM image, the shortest possible route and the entropy values of the images are obtained using Critical Path Methodology during the implementation of Hybrid ACO.

The population set of the ants which is an empirical value, based on the resolution of the image segregated into two categories as real and virtual ants helps in detecting the edge of the image based on the intensity values of each pixels, It traverses across the entire image with the concept of 8-pixel neighborhood and considering the intensity values on all the 8 neighborhood cells from the current pixel cell. This is done once exactly in the by an ant during the iteration monitored by the Method functions in ACO. The chromosomes are assigned with different permutation values from 1 to n in the GA, as the number of pixels traversed by the ant will be based on the order of their visit to each every local pixel/cell in the image. We also assume that the ant traversing path is restricted to the resolution of the image and thus the distance between the pixels are considered to be fixed values as C_i and C_j, where i,j ϵ n. This is considered to be a closed combinatorial problem well within the prescribed resolution of the image, considered as the boundary.

The chromosome value representing the solution to the problem is being solved by the GA. Each solution in the array is encoded as an array and is processed for optimization by the GA. The problem with N_{par} dimensions are encoded as N_{par} element array, as in

chromosome = $[p_1, p_2, \ldots, p_{Npar}]$

Here in the above expression, the parameter values are devised as per the specification of the problem as chromosomes. Each parameter value is converted into bit string making suitable for digital imaging solutions across the combinatorial problem solving algorithm, as in DICOM image fitness value calculation and image enhancement. The GA implemented in this paper uses the randomly chosen chromosomes and is evaluated for the fitness value by the fitness function to make it suitable of solving the combinatorial problem. The selection operator in the GA chooses the chromosome for reproduction based probability distribution, p_c. The equation that monitors this distribution is as given below,

$$P(C) = \left| \frac{f(C)}{\sum_{i=1}^{Npop} f(Ci)} \right|$$

The selection operator chooses the replacement for the chromosomes and this might allow for the same chromosome to be chosen more than once. The crossover operator recombines the chromosomes by swapping the chosen chromosomes and creates off-springs. The mutation operator randomly flips individual bits in the bit string of the newly generated chromosome. The mutation probability is also considered here in this case. This is monitored by setting the suitable value for p_m. Preference of calling the operators like, selection before the crossover can be set. Selection and crossover operators reproducing the newer chromosomes reproduce only fitter chromosomes making the GA to converge with an optimized solution too quickly. Thus the algorithm can also stop at the local optimum before the global optimum. This is overcome with the help of the mutant operator which helps in maintaining the diversity and integrity among the chosen population.

The initial population corresponding to the initial off-springs produced by the operators like selection, crossover and mutation by GA will be replaced with a new set of off-springs by the initial off-springs. This is repeated upon each iteration cycle and will be continued until the global optimum solution is obtained. The next new generation of chromosomes produced is tested by the fitness function. This is repeated for each generation. The iterations repeat till the GA produces the chromosomes with best fit

values and the fitness value stabilizes and does not change for generations reproduced by the new chromosomes. The factors such as probability of crossover, mutation probability and the size of the population are being considered. The methodology involved in GA uses traditional search methods, within the search space to obtain optimized solutions.

i. ***Search for stored Data –*** Retrieving the stored information from the storage device has to be precise. The binary search methodology befits the efficient and effective way of searching the correct binary data and analysis.

ii. ***Search for paths to achieve optimized results –*** This search methodology is similar to the methodologies opted in various artificial intelligence algorithms. A partial search tree kind of a structure is formed which guides I searching for the best fit solution. The root of the tree represents the initial state while the nodes branching out represent all the possible results with its updating from one state to another. This also resembles as the methodology for identification of the shortest path.

iii. ***Search for solutions - This*** is more suited for GA wherein the search for the solutions subsumes the search for the path in identifying the best optimized solutions. The proposed algorithm is as shown below in Table 1.

Table 1 Genetic Algorithm Workflow

1. ***Input bitmap image (.bmp)***
2. ***Set the population size to that of the image resolution bounds, as round($\sqrt{rows * columns}$) of the input image***
3. ***Set the probability of the crossover, $p_c = 0.8$***
4. ***Set the probability of mutation, $p_m = 0.08$ (Note this must be minimal)***
5. ***Set the chromosome length to obtain an optimized solution***
6. ***Initialize the population size and the chromosome length***

For the size of the chosen population

Apply the operators

   i. ***Selection***
   ii. ***Crossover***
   iii. ***Mutation***

7. ***Calculate the fitness values for the operators***
8. ***Update the initial generation with the new chromosomes***
9. ***Find the best fit solution***

The operators of GA are modified as functions and are as shown in the Table 2 and Table 3.

Table 2 Mutation Workflow

1. *New population is updated with mutation*
2. *The initial generation of chromosomes are assumed to be fit by set it to all ones*
3. *The mutants are generated randomly as suggested for reproduction*
4. *The new population is updated with new chromosomes*
5. *Else the population is updated with the ones, as taken with the previous population*

Table 3 Crossover Workflow

1. *For the size of the image bounded by its resolution, set the population values initially as ones.*
2. *The random length combination of the chromosomes are performed*
3. *If the randomly selected value is less than the probability of the crossover p_c, then the new population is obtained by crossover*
4. *Else it remains as the old population size*
5. *The crossover across on randomly selected chromosomes among the population*

5 Analysis and Results

The proposed algorithm is applied for the DICOM image, a CT scan image of the human brain. The image is processed with generic Ant Colony Optimization and Hybrid ACO-CPM algorithms. The processed image files are subjected to GA for finding the best fit solutions and fitness values obtained from number of iterations as outputs. The fitness values are compared among the images obtained with the application of the methods such as Sine, Gaussian, Fourier and Wave in the ACO and the Hybrid ACO-CPM. But in Hybrid ACO-CPM the ant population is segregated into two categories as real and virtual ants. The image edge processed by real ants is considered as input by the virtual ants and the image edge is linearly covered for the uncovered regions. A figure-of-merit is constructed based on the image analysis, fitness values and the best fit values are plotted for comparison.

Figure 1 Original Bitmap Brain Image

Figure 2 Hybrid ACO-CPM processed Images by Real Ants

Figure 3 Hybrid ACO-CPM processed Images by Virtual Ants

The GA is run for accessing and evaluating the fitness values and best fit value. With the fitness values compared for the edge processed DICOM images and the Best fit value to be considered being minimal suits the best possible solution. The images below represent the Fitness Values and Best fit value plots for original image processed by generic ACO and Hybrid ACO-CPM. This helps in evaluating the need for image enhancement and its inherent characteristics via figure-of-merit.

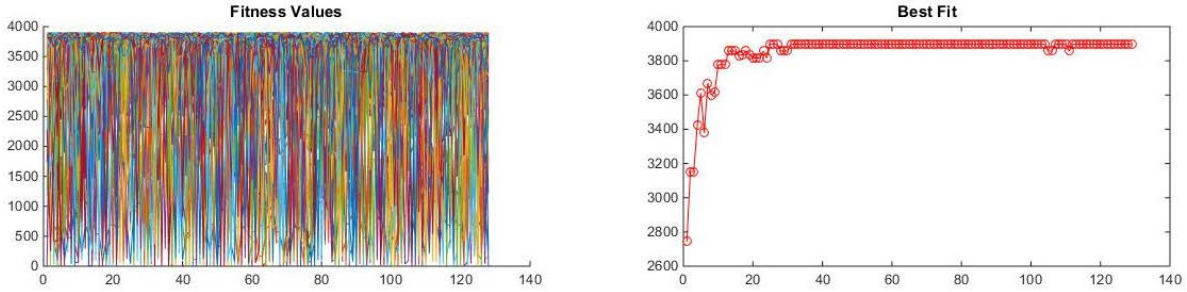

Figure 4 Fitness Values and Best Fit Value for the image processed with ACO algorithm

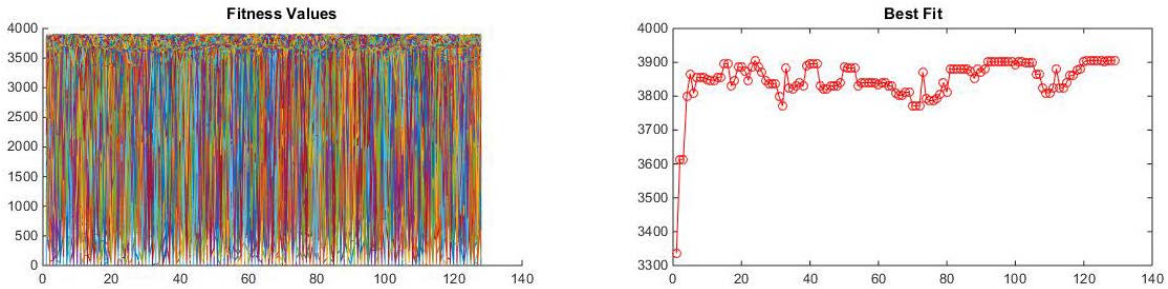

Figure 5 Fitness Values and Best Fit Value for the image processed with Hybrid ACO-CPM algorithm for Real Ants

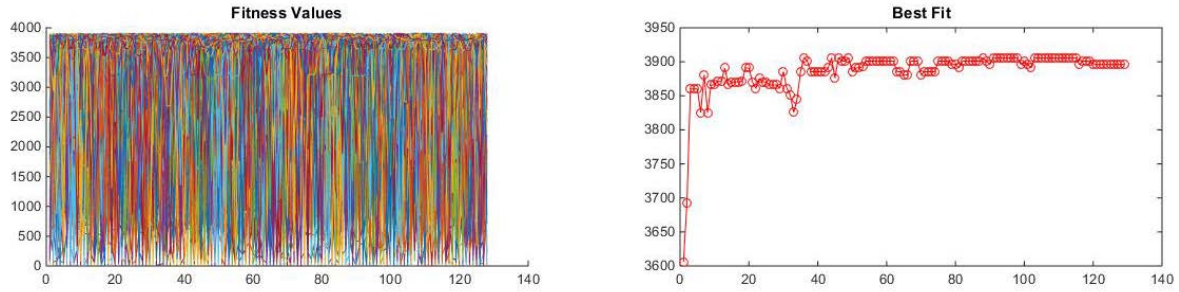

Figure 6 Fitness Values and Best Fit Value for the image processed with Hybrid ACO-CPM algorithm for Virtual Ants

Figure-of-Merit

The figure-of-merit helps us in finding the deviations between the algorithms used in detecting the edge of DICOM image and its application. It also helps in evaluating the efficiency of the algorithm. The fitness values computed using the GA and the image enhancements factors helps in differentiating and analyze the productivity of the algorithm as proposed in Hybrid ACO-CPM, with the generic ACO algorithm. This also shows the deviations among various algorithms, wherein the image solutions being optimized across at different fitness value rates versus the population size. In this case and for the considered DICOM image, it's the pixel count.

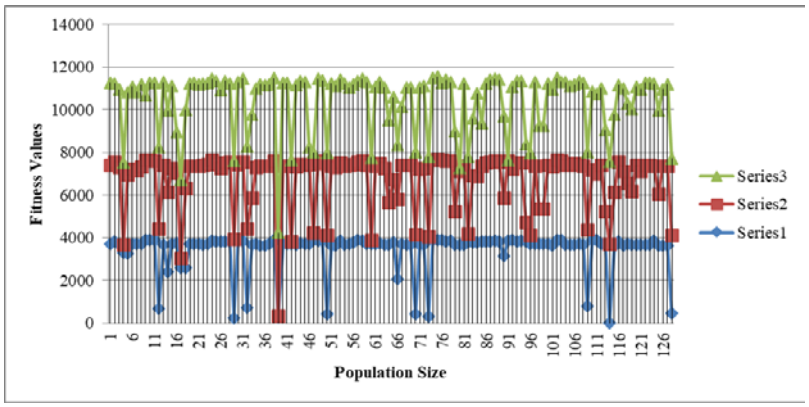

Figure 7 Figure-of-Merit with the Fitness Values vs Population Size

In the above figure the Series 1 corresponds to the fitness values obtained from the DICOM image processed by Hybrid ACO-CPM with virtual ants. While Series 2 corresponds to the fitness values obtained by processing the DICOM image using Hybrid ACO-CPM with real ants. Series 3 corresponds to the fitness values obtained from the DICOM image processed by generic ACO algorithm. The optimization is inferred from the plot wherein the more linear values are intended to be most optimized with the application of GA.

6 Conclusion

The solutions to the combinatorial problems like the edge detection within a DICOM image using the Hybrid ACO-CPM algorithmic approach are dynamic and they evolve with the dynamics of the image. The reliability of these algorithms rendering an optimized solution from a set of solutions is much desirable from the optimization algorithm. Also the need for a better visual quality image after the processing by the edge detection optimization algorithms enhance the diagnosis capabilities with the

DICOM standard medical image. This purpose of image enhancement with the provision of an optimized solution from a collection of solutions is successfully taken care by the application of Genetic Algorithms. The evolution also plays an important role in obtaining new population as well as much better optimized results from the search space of the solutions to the problem.

In this paper, we could successfully implement the GA for the DICOM images processed by generic ACO and as well as for Hybrid ACO-CPM. The figure-of-merit is plotted and analyzed to evaluate between the different implementation features and characteristics of these edge detection algorithms. Also the impact of these algorithms is analyzed with the application of GA on the images obtained from these algorithms. The evaluation resulted in proving that the Hybrid ACO-CPM is more suitable with an optimized solution within the entire search space of solutions. This also shows that the convergence rate of the solutions is much faster and more adaptable with the increase in the population count.

REFERENCES

[1] Davis, L., Ed. (1987), Genetic Algorithms and Simulated Annealing, Pitman, London.

[2] Goldberg, D .E. (1989), Genetic Algorithms: Search, Optimization and Machine Learning. Addison Wesley, Reading, MA.

[3] Whitley D. A genetic algorithm tutorial. Statistics and computing. 1994 Jun 1;4(2):65-85.

[4] Derrac J, García S, Molina D, Herrera F. A practical tutorial on the use of nonparametric statistical tests as a methodology for comparing evolutionary and swarm intelligence algorithms. Swarm and Evolutionary Computation. 2011 Mar 31;1(1):3-18.

[5] S. Chetan, H.S. Sheshadri, V. Lokesha, "A Hybrid Critical path methodology - ABCP (As Built Critical Path); its Implementation and Analysis with ACO for Medical Image Edge Detection", International Journal of Computer Science, Information technology and Control Engineering (IJCSITCE), Vol.2, No.1/2, April 2015, pp.27 - 42, ISSN: 2394-7527.

[6] Dorigo M, Birattari M, Stutzle T. Ant colony optimization. IEEE computational intelligence magazine. 2006 Nov;1(4):28-39.

[7] Ankerbrandt, C.A., B .P . Unckles and F.E. Petry (1990) Scene recognition using genetic algorithms with semantic nets, Pattern Recognition Left , 11, 285-293.

[8] Siedlecki W. and I . Sklansky (1989), A note on genetic algorithms for large-scale feature selection. Pattern Recognition Lett. 10. 335-347.

[9] Proceedings of the Fourth Internal. Conf. on Genetic Algorithms (1991), University of California, San Diego.

[10] Pal SK, Bhandari D, Kundu MK. Genetic algorithms for optimal image enhancement. Pattern Recognition Letters. 1994 Mar 1;15(3):261-71.

[11] Shivangini Shrivastava, Arvind Upadhyay, "Image Enhancement using Genetic Algorithm", Internaltional Journal of Engineering Research & Technology (IJERT), Vol.3, Issue 5, May 2014, pp.1768-1772. ISSN: 2278-0181.

[12] Palanikumar S, Sasikumar M, Rajeesh J. Entropy optimized palmprint enhancement using genetic algorithm and histogram equalization. International Journal of Genetic Engineering. 2012;2(2):12-8.

[13] Hole KR, Gulhane VS, Shellokar ND. Application of genetic algorithm for image enhancement and segmentation. International Journal of Advanced Research in Computer Engineering & Technology (IJARCET). 2013 Apr 28;2(4):pp-1342.

[14] Kaur A, Jindal G. Overview of tumor detection using genetic algorithm. International Journal Of Innovations In Engineering &Technology (IJIET) Vol. 2013 Apr;2.

[15] Katkovnik V, Egiazarian K, Astola J. Local approximation techniques in signal and image processing. Bellingham: SPIE.

SOCIETY FOR SCIENCE AND EDUCATION UNITED KINGDOM

JBEMi JOURNAL OF BIOMEDICAL ENGINEERING AND MEDICAL IMAGING

ISSN: 2055-1266
VOLUME 4 ISSUE 4

Finger Movement Identification Using EMG Signal on the Forearm

[1]N. Sheikh, [1]F. Muhammad, [2]M. F. Shamim, [1]N. Shahid, [1]S. M. Omair, and [1,2]M. Z. Ul Haque
[1]Biomedical Engineering Department, Sir Syed University of Engineering and Technology, Karachi, Pakistan;
[2]Department of Biomedical Engineering, Barrett Hodgson University, Karachi, Pakistan;
naeem_sheikh23@hotmail.com; fyda.fydai@hotmail.com; fahadshamem@gmail.com; engr.nageenshahid@gmail.com; smomair@ssuet.edu.pk; muhammad.zeeshan@bhu.edu.pk

ABSTRACT

Finger movement identification is an important innovative interfacing method which has countless possible applications. It can be used to create a new age in human computer interfacing (HCI) devices. It can also be applied to medical applications, such as in the development of a more advanced prosthetic hand. The current research for this purpose includes methods such as computer vision and detecting finger motion through mechanical vibrations from skin surface. They have the limitation of being restrictive, in terms of the degree of movement that the hand is allowed from a certain optimum position, as well as being susceptible to environmental factors. In this study, the surface electromyography (sEMG) of the forearm from skin electrodes is developed and interfaced with computer. The response at the flexor carpi radialis muscle of the forearm is plotted for a group of subjects to observe the qualitative responsiveness of the sEMG to different types of finger movements. The results show that finger movement generates a corresponding response on the EMG electrodes. For the particular muscle being studied, the greatest individual digit amplitude response was observed for the ring finger (digitus annularis) across the subjects. In future studies, this research could be made more quantitative in nature by observing the frequency content of a variety of hand gestures across a sample of subjects.

***Keywords*:** Human computer interfacing; finger detection; surface electromyography; finger movement; flexor carpi radialis; digitus annularis.

1 Introduction

Recently, detection of finger movement has been gaining increasing attention as a new method for human computer interfacing (HCI) [1]. Examples of areas where this can be applied are augmented reality, active prosthetics, playing video games, and controlling particular devices. They can be improved to have a more user friendly implementation through new and novel methods of HCI such as finger gesture recognition [2-4]. Humans interact with computers in different ways, amongst which, the mouse is one of the most widely used methods. The mouse has, in essence, a very simple mechanism, which does not really require the array of complex motions that many of the studies related to finger detection

DOI: 10.14738/jbemi.44.3528
Publication Date: 17th August 2017
URL: http://dx.doi.org/10.14738/jbemi. 44.3528

exhibit. An alternative to the mouse could be simple as individual finger detection. For this, surface electromyography (sEMG), in particular, of the forearm, is an important avenue of research to classify and differentiate each digit of the hand and can then be used by users to communicate with devices.

Kulshreshth et al. used Microsoft Kinect as an input device to track fingers in real-time. The image was processed through algorithms to detect fingers by matching them to various templates to classify them [5]. The technique's accuracy was restricted by the limited resolution of the Kinect, which meant that accuracy of the finger detection decreased as the user moved his hand away from the Kinect. Aside from this issue, the orientation of the hand was also limited, as it needs the hand to be parallel to the camera plane with the fingers at a distance from each other.

Kishi et al. applied accelerometers to detect mechanical vibration patterns to detect finger motion while fingers were tapping [6]. Sensors are placed on the forearm of the subject. The difference between each finger in amplitude and frequency was indiscernible, so they then used template matching method to identify each digit of the hand. The success rate of identifying finger motion was relatively high; however, use of accelerometer sensors would be heavily prone to external artifacts, such as an external force applied on the forearm could disturb the readings. A big limitation of this method is that the finger motion detected is limited to finger tapping, which limits the degree of freedom for the hand.

Using electromyography to detect finger movements is not a new idea; rather, it is something that has been done in a variety of ways before as well. Previous studies used an EMG sensor device to integrate changes in muscle potential due to finger movement to a computer interface [7-11]. These can be in varying arrangements with different methods of classification such as using neural networks to train and classify a system to correctly identify a particular finger according to the data received from the EMG device.

In this study, the data from previous work is considered and brings up the question of whether the classification of the fingers can be achieved using only a single pair of electrodes rather than using a multiple sensor configuration. Also, if this can be achieved without the use of algorithms, neural networks and other such methods. In this study, an EMG sensing device using a single pair of surface electrodes was designed first, and then, finger movement is detected by placing the surface electrodes on the flexor carpi radialis muscle of 11 subjects. This was done to observe the response of different finger movements across the different subjects. The site of electrode placement was chosen as superficial area above the belly of the flexor carpi radialis muscle. The electrode distance was kept constant in all subjects as 25 mm. The subjects were prompted to do opening (extension) and closing (flexion) finger movements and the resulting sEMG signals were recorded and stored on a computer.

2 Methodology

The various system components for sensing changes in sEMG signal are shown in Figure 1. After acquiring a sEMG signal, qualitative observations of the sEMG signals of 11 subjects is taken while they open and close different fingers when prompted.

2.1 Electrodes

In this work, three disposable EMG surface electrodes are used per subject. Two of the electrodes are placed at the muscle of interest (flexor carpi radialis) at a distance of 25 mm from each other. The placement of the electrodes was within the range of inter-electrode distance used for kinesiological

electromyography [12]. The electrodes are placed at the same muscle across all the subjects [4, 13]. A reference electrode is placed on the styloid process of the radius [12].

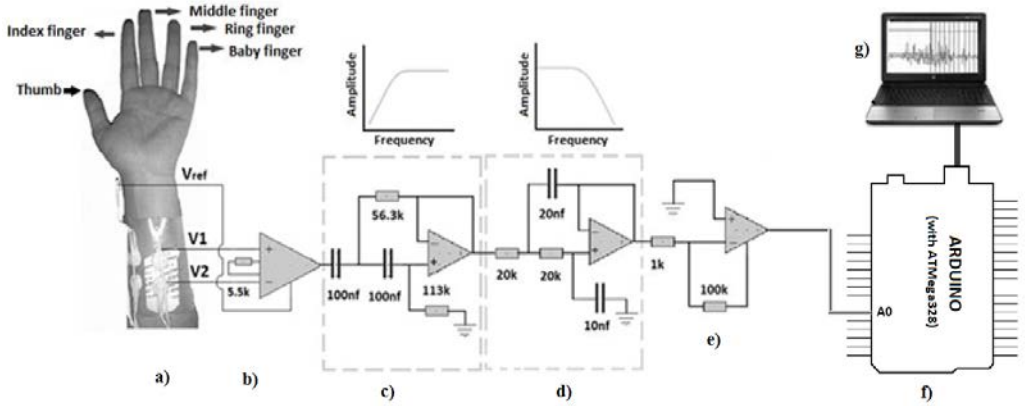

Figure. 8: System Components. (a) Forearm with electrodes placed on muscle of Interest. (b) Pre-amplifier. (c) High-Pass filter. (d) Low-pass filter. (e) Gain amplifier (f) Microcontroller. (g) Computer with software for plotting and storing EMG data.

2.2 Preamplifier

The human body has high impedance. This requires a preamplifier so that current is not drawn from the body. In this study, an instrumentation amplifier, INA114 [14], is used to amplify the incoming signals from the electrodes by a factor of 10 before the filtering phase.

2.3 Filter

For surface EMG, the frequency contents are generally considered anywhere in between the range of 0 to 500Hz [12, 15]. In this work, we implement a second order; band-pass filter from 20 to 500Hz using LM358 [16], the lower cut-off frequency is considered 20Hz, rather than 0Hz to remove baseline noise. A notch filter for the 50 Hz power line is not used as experts discourage its use, as it removes important EMG information along with the noise [15].

2.4 Amplifier

Without any conditioning, sEMG signals amplitude range from ± 5mV [12]. Although, preamplifiers amplify the signal, dedicated amplifier stages are used to amplify the signal with a much higher gain setting. A two-stage amplifier using LM358 [16], with an overall gain of 100, is used in this work to bring the conditioned EMG signal to range across 0 to 5V.

2.5 Data Acquisition

To Interface the signals with the computer and to convert the signal from analog to the digital form, an ATMega328 is used [17]. ATMega328 has a 10-bit analog to digital converter. In this experiment, pin 23 of this microcontroller is used to provide analog to digital conversion of the data. By itself, the microcontroller can't relay the data to the computer, so, it is used in conjunction with an Arduino Uno board. The Uno board allows for interfacing with a computer and even emulating a virtual COM port for serial communication over USB using an ATmega16U2 on board. Programming of the microcontroller was done using the Arduino IDE, which has C-language based syntax.

2.6 Data Display/Storage

Serial communication through USB is used to relay data to the computer. Communication is done at a Baud rate of 115200 bits per second. The visualization of data and storage is possible through a graphical program built in the processing IDE. The program emulates an oscilloscope taking the amplitude at each sample and plotting it as a graph. It also saves the data for further processing offline.

After development of this sensor circuitry and interfacing it with signal graphing program, we have taken observations on 11 male subjects aged between 22 – 25 years, who have electrodes placed on their left arms. The muscle being studied in this work was the flexor carpi radialis and an inter-electrode distance was fixed at 25 mm. The electrodes are placed at the belly of the muscle [18]. Each subject is prompted to perform flexion and extension of each finger one by one. The data is visually displayed in real time on the computer and then, every 10 seconds the EMG data of the subject is saved.

3 Results and Discussions

The sample graphical results for one of the subjects using our sEMG sensing circuit are shown in Figure 2. In Figure 2(a), it can be seen that the thumb shows no response. This is due to the muscle that can be studied to detect flexion of thumb finger, the flexor pollicus longus is quite distant from the flexor carpi radialis muscle and has no contact with it either, making it isolated, leading to the no response readings in each subject. The index finger showed a relatively low response, as seen in Figure 2(b). This can be explained, as the muscles responsible for flexion of index finger, the flexor digitorum superficialis is distant from the site of electrode placement, but can still have some effect as it is surrounding the muscle being observed in this study. A mid-level response is observed for the middle finger shown in Figure 2(c). This can be explained as the location of electrode placement is extremely near to the muscles in question, which is responsible for detection of flexion of the middle finger, the flexor carpi radialis and palmaris longus. Figure 2 (d) shows the subject highest relative response with ring finger contraction. This was because of the flexor carpi radialis muscles directly responsible to detect the flexion of the ring finger [4]. Like this, the baby finger shows a relatively low response, on average, as can be noted in Figure 2 (e). Similar to the index finger, the muscle responsible for flexion of baby finger, the flexor carpi ulnaris is also distant from the site of electrode placement, but can still have an effect on the electrodes placed on flexor carpi radialis.

In studies like this, quantitative data collection of the EMG signals of each subject is unfeasible, as many factors make it impossible to reproduce the same results in subsequent trials. For example, one factor is electrode placement, which is difficult to get at the exact same location and even minute changes in position or inter distance can change the amplitude of the signal greatly. As such, even on the same subject, if the subject is tested once, and then, at a later time, examined again, quantitatively, the results will not be the same due to the factors mentioned previously. As such, the better option is to take qualitative observations of the signals at the muscle site to check the trend of the EMG signal amplitudes is done. These readings are observed and noted down, which can be studied in Table 1.

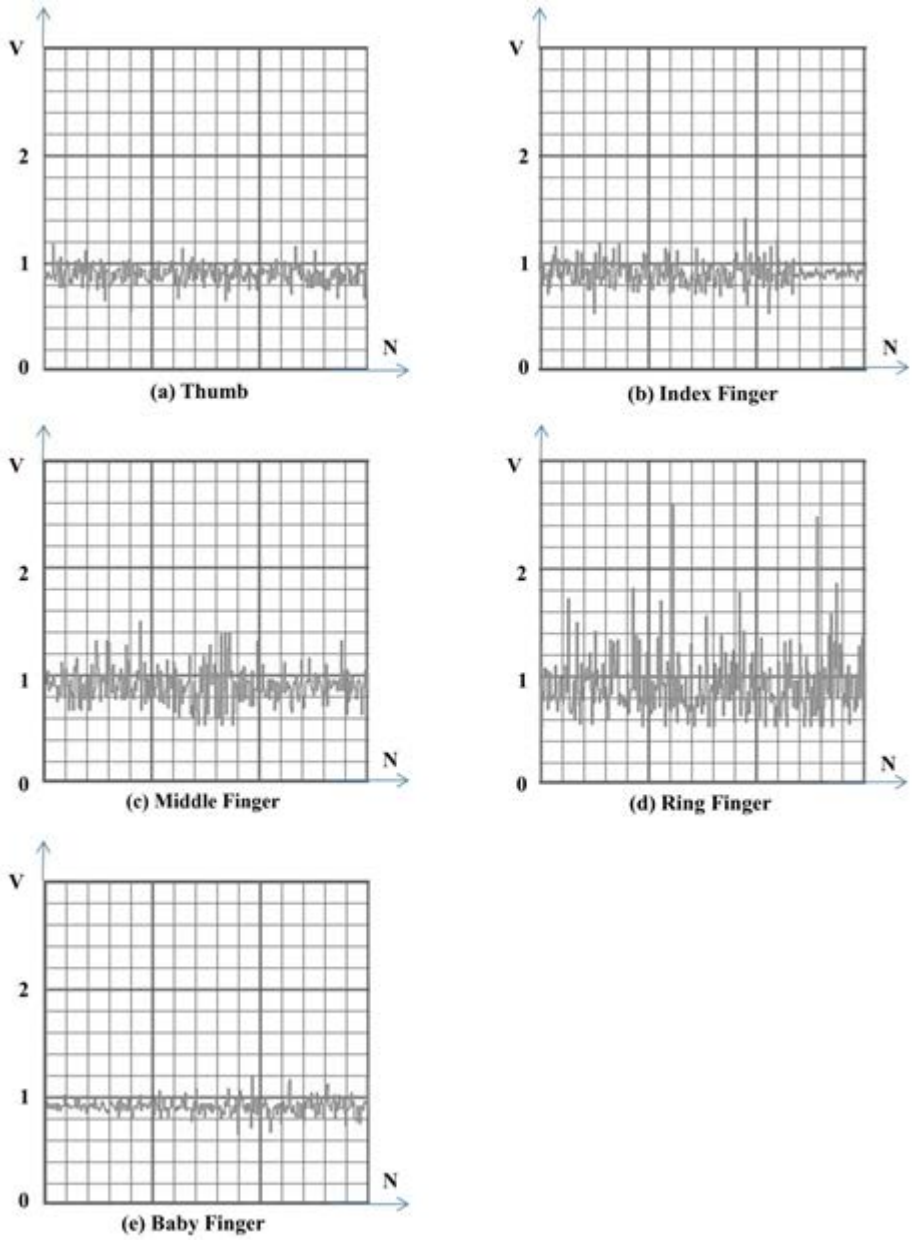

Figure.9.sEMG graphs corresponding to Finger movement with x- axis shows the number of samples taken in N, and y-axis shows the voltage in V

Table 1 listed the relative amplitude intensity of each individual digit of the different subjects. Table 1 shows some fluctuations in the readings, in particular, the readings of the index, middle and baby finger. This variation from subject to subject can be explained by minute differences in electrode placement. It is humanely impossible to get the same exact position for each subject, due to human error, differing arm size, amongst other factors. As such, the electrodes can be placed at a position in which the main muscle being studied is still detected correctly, however, the surrounding muscle which also have effects on the sEMG signal observed are not picked up as well by the electrodes, when moving from subject to subject. The observations revealed that amongst all the samples taken for each subject, flexion of the ring finger (Digitus annularis) consistently managed to have the highest amplitude relative to the other

digits of the hand. The middle finger was relatively constant amongst the subjects, giving a response that could be easily distinguished from the higher amplitude ring finger and the other digits. The thumb gave no visible response whatsoever, whereas the index and baby fingers gave a low level response. This confirms that the flexor carpi radialis muscle is responsible for detection of ring finger flexion primarily. Also, the muscles surrounding it, which are also responsible for finger detection can, also have a resultant effect, although of a much lesser amplitude.

Table 1: Relative amplitude intensity of each individual digit of the different subjects

Sample	Thumb	Index	Middle	Ring	Baby
A	No response	Low	Intermediate	High	Low
B	No response	Intermediate	Low	High	Low
C	No response	Low	Low	High	Low
D	No response	Low	Intermediate	High	Low
E	No response	Intermediate	Intermediate	High	Low
F	No response	Low	Intermediate	High	Low
G	No response	Low	No response	High	No response
H	No response	No response	Intermediate	Intermediate	No response
I	No response	Low	Intermediate	High	Low
J	No response	Low	Intermediate	High	No response
K	No response	Intermediate	Intermediate	High	Low

Where; No Response = No response, Low = Low amplitude response, Intermediate = Intermediate level response and High = High level response.

The observations show that even while using a single pair of electrodes, the different fingers respond differently when flexed. Visually, they can be distinguished by the amplitude intensity each digit exhibits when closed, which is different for each finger. At the flexor carpi radialis, the highest response was observed for ring finger, which was constant across all the subjects. Whereas there was some variation between the results for the other fingers when changing from subject to subject, on average it could be determined that the thumb showed no response, the index and baby fingers gave low level responses and the middle finger gave an intermediary response. Amongst the index and baby fingers, the maximum amplitude reached is similar between the two, which would be hard to distinguish from each other for the devices. Also since thumb gave no response, it cannot be determined at the particular site we chose to place electrodes on. However, it is quite feasible to distinguish the other fingers due to the intensity difference amongst the fingers.

4 Conclusions

In this study, the finger movements of different subjects were observed and analyzed by plotting their sEMG at the forearm, using a single pair of electrodes, placed above the flexor carpi radialis. It was noted that different fingers gave different EMG amplitude in response to finger movement when monitored from the same electrode site. However, the change in amplitude in detecting the different fingers flexion was relatively same throughout the study. At the Flexor carpi radialis muscle, the ring finger gave the highest individual finger response. Other fingers also showed responses, albeit, less intense as compared to that of the ring finger. This study could be made more comprehensive by taking signal analysis on different forearm muscles or by repeating the study while having an array of electrode

pairs around the forearm, integrating the information from each electrode pair during gesture detection for a more detailed response analysis to each individual finger. It can be further improved by implementing digital filters to remove noise and artifacts better. In the future, a study using frequency analysis of the signals could give more detailed information on classifying fingers using EMG, as the information gathered by frequency analysis can be studied quantitatively and can then be further assessed to formulate a strong relationship which can correlate the response that each finger flexion generates to the site of electrode placement. By applying all these modifications and future advancements, a collection of gesture templates can be generated, starting from simple single finger gestures to complex gestures, involving all the fingers. These templates can then be used to reliably detect a multitude of different gestures, using sEMG signals.

REFERENCES

[1] M. K. Bhuyan, K. F. MacDorman, M. K. Kar, D. R. Neog, B. C. Lovell, and P. Gadde, "Hand pose recognition from monocular images by geometrical and texture analysis," *Journal of Visual Languages & Computing,* vol. 28, pp. 39-55, 2015.

[2] M. M. Hasan and P. K. Mishra, "Comparative Study for Construction of Gesture Recognition System," *International Journal of Computer Science and Software Technology,* vol. 4, pp. 15-21, 2011.

[3] A. Andrews, "Finger movement classification using forearm EMG signals," 2008.

[4] S. Maier and P. van der Smagt, "Surface EMG suffices to classify the motion of each finger independently," in *Proceedings of MOVIC 2008, 9th International Conference on Motion and Vibration Control*, 2008, pp. 15-18.

[5] A. Kulshreshth, C. Zorn, and J. LaViola, "Real-time markerless kinect based finger tracking and hand gesture recognition for HCI," in *Proceedings of the IEEE Symposium on 3D User Interfaces (March 2013)*, pp. 187-188.

[6] T. Kishi and W. Yu, "Finger motion recognition by skin surface vibration patterns," *Int J Bioelctromagnet,* vol. 9, pp. 48-9, 2007.

[7] T. S. Saponas, D. S. Tan, D. Morris, and R. Balakrishnan, "Demonstrating the feasibility of using forearm electromyography for muscle-computer interfaces," in *Proceedings of the SIGCHI Conference on Human Factors in Computing Systems*, 2008, pp. 515-524.

[8] M. Gazzoni, N. Celadon, D. Mastrapasqua, M. Paleari, V. Margaria, and P. Ariano, "Quantifying forearm muscle activity during wrist and finger movements by means of multi-channel electromyography," *PloS one,* vol. 9, p. e109943, 2014.

[9] L. J. Hargrove, K. Englehart, and B. Hudgins, "A comparison of surface and intramuscular myoelectric signal classification," *IEEE Transactions on Biomedical Engineering,* vol. 54, pp. 847-853, 2007.

[10] A. Jennifer Keating, "Relating Forearm Muscle Electrical Activity to Finger Forces," Master of Science Thesis, Faculty of the Worcester Polytechnic Institute, Worcester Polytechnic Institute, 2014.

[11] G. Tsenov, A. Zeghbib, F. Palis, N. Shoylev, and V. Mladenov, "Neural networks for online classification of hand and finger movements using surface EMG signals," in *2006 8th Seminar on Neural Network Applications in Electrical Engineering*, 2006, pp. 167-171.

[12] V. Medved and M. Cifrek, *Kinesiological electromyography*: InTech, 2011.

[13] V. Florimond, "Basics of surface electromyography applied to physical rehabilitation and biomechanics," *Montreal, Canada: Thought Technology Ltd,* 2009.

[14] I. P. I. Amplifier, "Burr–Brown Corporation," *USA, March,* 1998.

[15] E. A. Clancy, "Design of a High–Resolution Surface Electromyogram (EMG) Conditioning Circuit," WORCESTER POLYTECHNIC INSTITUTE, 2012.

[16] T. Instruments, "LM358 Datasheet," staženo 2014-02-27. http://www.ti.com/lit/ds/symlink/lm158-n.pdf

[17] A. Coorporation, "Atmel ATmega328P Datasheet," ed, 2011.

[18] G. S. Rash and P. Quesada, "Electromyography fundamentals," *Retrieved February,* vol. 4, 2003.

SOCIETY FOR SCIENCE AND EDUCATION UNITED KINGDOM

JBEMi JOURNAL OF BIOMEDICAL ENGINEERING AND MEDICAL IMAGING

ISSN: 2055-1266
VOLUME 4 ISSUE 4

Automated Pulmonary Lung Nodule Detection Using an Optimal Manifold Statistical Based Feature Descriptor and SVM Classifier

[1]Ammi Reddy Pulagam, [2]Venkata Krıshna Rao Ede, [3]Ramesh Babu Inampudi
[1]Vasireddy Venkatadri Institute of Technology, Nambur, Guntur, AP, India;
[2,]Lakireddy Bali Reddy College of Engineering, Mylavaram, Vijayawada, AP, India;
[3]Acharya Nagrjuna University, Nagarjuna Nagar Guntur, AP, India;
pulagamammireddy@gmail.com; krishnaraoede@yahoo.co.in; rinampudi@hotmail.com

ABSTRACT

The pulmonary lung nodule is the most common indicator of lung cancer. An efficient automated pulmonary nodule detection system aids the radiologists to detect the lung abnormalities at an early stage. In this paper, an automated lung nodule detection system using a feature descriptor based on optimal manifold statistical thresholding to segment lung nodules in Computed Tomography (CT) scans is presented. The system comprises three processing stages. In the first stage, the lung region is extracted from thoracic CT scans using gray level thresholding and 3D connected component labeling. After that novel lung contour correction method is proposed using modified convex hull algorithm to correct the border of a diseased lung. In the second stage, optimal manifold statistical image thresholding is described to minimize the discrepancy between nodules and other tissues of the segmented lung region. Finally, a set of 2D and 3D features are extracted from the nodule candidates, and then the system is trained by employing support vector machines (SVM) to classify the nodules and non-nodules. The performance of the proposed system is assessed using Lung TIME database. The system is tested on 148 cases containing 36408 slices with total sensitivity of 94.3%, is achieved with only 2.6 false positives per scan.

Keywords: computed tomography, lung cancer, pulmonary nodules, statistical thresholding, SVM.

1 Introduction

Lung Cancer is one of the prime causes of death related to cancers at global level. Majority of the patients suffering from lung cancer are at advanced stage (stage IV – 40%, stage III – 30%), and only 16% survival rate for the present five years is found [1]. Identification at an early stage and initiating the treatment for the lung cancer can significantly improve the survival rate of the patients. Computed Tomography (CT) is the most accurate imaging modality available for early detection and diagnosis of lung nodules (cancer). It can be used to detect pathological deposits even smaller than 1 mm in diameter. The nodule is a round or irregular opaque shape with a diameter up to 30 mm on a CT scan. Early detection of nodules is a vital step in diagnosing the lung cancer, but CT scan comprises large quantity of images which is time consuming for the radiologist to assess. In this connection, the computer aided detection (CAD) is a remedy that can provide an effective solution by assisting the

DOI: 10.14738/jbemi.44.3354
Publication Date: 30th Aug 2017
URL: http://dx.doi.org/10.14738/jbemi.44.3354

radiologists with significantly improving the scanning efficiency for visualization, detection and characterization of nodules [2, 3]. In this light we present an automated pulmonary lung nodule detection system from CT images on a slice method in this paper. Once the nodules have been detected in each slice, a 3D surface of the nodule can then be reconstructed. Our method allows, naturally an extraction of pulmonary lung nodule candidates which can further be used to classify the nodules.

2 Previous Work

For over a decade, scholars from various strata of the globe have put forward a series of pulmonary lung nodule detection methods [4-21]. The primary stages employed in these lung nodule detection methods are lung segmentation [4-13], nodule candidate detection [14-19], and elimination of false positive nodules (FPNs) [10, 14, 19-21]. The first stage shows that lungs look like dark regions in CT scans, as they are basically bags full of air inside it, hence, the image intensities of the lung and surrounding tissues are clearly contrasted. This phenomenon encouraged good number of researchers to search for an effective thresholding method which can separate the lung region from all other tissues. A threshold to extract an initial lung region can basically be computed. Global thresholding is an effective technique for extracting the initial lung region as it segments the scans with distinctive gray levels relating to lung region and background [5-6]. Initial lung region can also be segmented using a fixed threshold [6-7], 3-D adaptive fuzzy thresholding [7], region growing [8] and hybrid segmentation [9]. In case of lung edge affecting pathologies, all these methods are found to be ineffective. This is because of the changes in image intensity at pathological regions as well as the gray levels which are closer to that of muscle, fat, or bone. To overcome these problems**,** a chain code representation method [10], morphological approaches [11], a rolling ball method [12] are used. In this paper a new contour correction method is proposed by using modified convex hull algorithm [13] for effective segmentation of lung region.

The second stage in lung nodule detection systems is the detection of lung nodule candidates. Multi gray level thresholding has been applied widely to identify nodule candidates [14]. Shape based template matching approach was used to detect the spherical nodules [15-16]. The 3D template matching approach utilizes 3D of regions of interest to identify structures having properties similar to pulmonary nodules [17]. The Filtering based method [18] detected the nodules by improving the intensity of nodules and reducing the same for non-nodules. In recent times, mass spring model based candidate detection method has been widely used to detect nodule candidates [19].These methods are unable to obtain satisfactory results, when lung regions having large variance discrepancy between the lung nodule and background. Hence, these methods consider only the class variance sum, but neglect the discrepancy of class variances. As an attempt to eliminate this limitation a new optimal statistical thresholding method is presented. This new method takes into account both the class variance sum and the variance discrepancy at the same time and constructs an optimal manifold statistical criterion for threshold selection within the region of interest (ROI).

The last stage in a lung nodule detection system is the classification of the lung nodules from non-nodules based on the extracted feature vectors from the segmented nodule candidates. Over the past decade, several methods [7, 10, 15, 20-21] have been proposed to reduce false positives. The rule-based filtering and linear discriminate analysis classifiers [5, 7, 12] are widely used for classification of nodule candidates. A rule-based filtering is only able to detect the general shape of nodules. A linear classifier cannot achieve acceptable results because the features extracted from nodule candidates are not linear.

Moreover, machine learning based detection methods have also been used for false positive reduction based on genetic algorithm, neural networks [14, 19], and genetic programming [20]. It should be noted that though the above classifiers comparatively large number of false positives are detected the still remain. In this paper we have used SVM classifier by radial basis function to classify pulmonary nodule detection to have improved accuracy and reduced false positive rate. The proposed system is evaluated using Lung TIME database [22] of thoracic CT scans with manually annotated pulmonary nodules. The experimental results have high degree of accuracy, sensitivity with reasonable specificity.

The remainder of this paper is organized in three major sections: In sub-section 3.1segmentation of lungs from the raw DICOM CT images is described. Sub-section 3.2 presents the extraction of nodule candidates from the segmented lung tissues. Classification of true nodules from the segmented nodule candidates is discussed in sub-section 3.3. Results of a detailed evaluation on 148 cases containing 36408 slices are presented in section 4. Conclusions are given in section 5.

3 Proposed Methodology

An overview of different stages of the proposed pulmonary lung nodule detection system is shown in Fig. 1.The basic objective of the first stage is to extract the lung region from the human chest CT scan which contain components like fat, other tissues (including trachea, fat, ribs, examination bed, and so on) and air-filled regions.

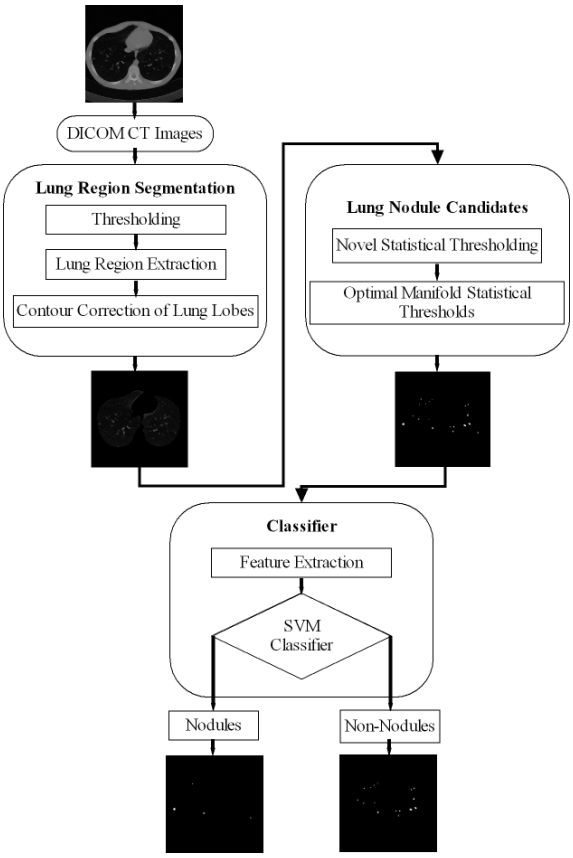

Figure.1 Process of proposed pulmonary lung nodule detection system

3.1 Lung region segmentation

The thoracic CT scan contains the lung parenchyma as shown in Fig. 2(a). The proposed lung region segmentation comprises three steps: (a) detection of binary lung mask using global thresholding, (b) Extraction of lung region employing 3D-connected component labeling and mathematical morphology and (c) refining the lung contour to get complete lung region using the proposed modified convex hull algorithm.

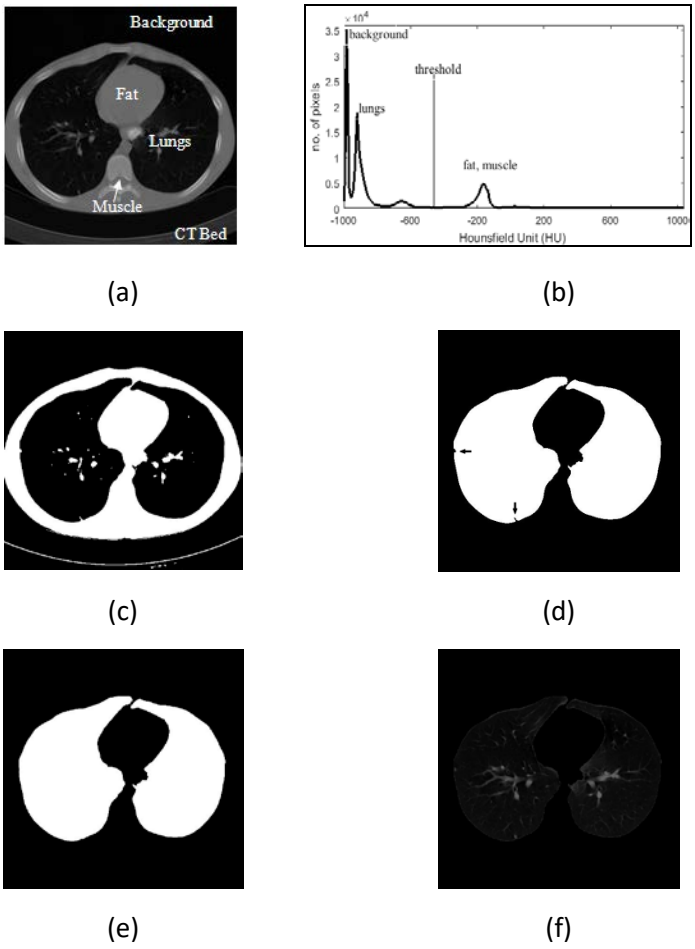

Figure. 2 (a) Original CT slice and tissues localization, (b) Threshold value selections based on histogram, (c) global threshold of (a), (d) Initial mask of lung region after removing background, fat, muscle, and CT bed, and mask after filling holes but it contains juxta-pleural nodules.(e) final mask after contour correction, (f) segmented lung region extraction

As the normal attenuation range for most of the lung tissue in a CT slice is from -910 HU to -350 HU. We set -350 HU as the threshold value for separating the lung region from the thoracic CT scan. Hence the initial lung mask is attained by thresholding all the non-body pixels which is given by

$$S_i(x,y) = Thr\ (f_i(x,y) - 350HU), \tag{1}$$

where $f_i(x,y)$ is a pixel at (x,y) for the input thoracic CT i^{th} slice of f. The initial lung mask obtained for the CT image is as shown in Fig. 2c.

In the initial lung masks obtained, black borders denote non-lung region and center black areas indicate the lung region. The non-lung regions are removed by flood filling. After that, 3D-connected component labeling is used to select largest and second largest labels that are lung regions and lung regions containing holes, which are normally vessels or nodules. Morphological hole-filling operations are applied to get binary lung mask as shown in Fig. 2(d).

If the CT slice contains juxta-pleural nodules along the contour of lung region, this will affect the detection of lung edges as the intensity of these nodules is same as that of the surrounding lung region. In this paper, a modified convex hull algorithm for the contour correction of lung region is presented.

The modified convexity algorithm is simulated from a fast algorithm for convex hull extraction in 2D image [13]. It initially finds the eight extreme points on the contour of binary image. The modified convexity algorithm extracts the extreme points by scanning the binary image from outer to inner. The boundary of the lung region is scanned pixel by pixel until it reaches the last boundary pixel. Thus, the monotone segments are obtained and the convex hull is extracted as presented in Fig. 3.

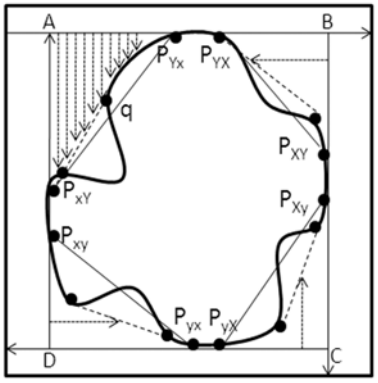

Figure.3 Extreme points (A: $P_{xY}P_{Yx}$, B:$P_{YX}P_{XY}$, C:$P_{Xy}P_{yx}$, and D:$P_{yx}P_{xy}$) of image convex hull and Scanned regions of image

The binary image is partitioned into four regions in Fig.3 (i.e. A P_{Yx} P_{xY} , B P_{XY} P_{YX} , C P_{yX} $P_{Xy,}$ and D P_{xy} P_{yx}) by employing these extreme points. Only these extreme points are processed while finding the vertex. By orderly monotone scanning increase then temporary convexity is extracted. The entire convexity is obtained by continuously improving the momentary convexity. These convex hull algorithm processes less storage space and time for scanned areas are less and only the vertices of temporary convexity require storage. After applying improved convex hull algorithm, the coarse segmented lung image is subtracted from the result of modified convex hull algorithm. As the resultant image contains some small responses and objects at the border, morphological erosion with a spherical kernel of size seven and connected label filtering are then applied to remove these responses. The eroded image is subtracted from the result of the modified convex hull algorithm to extract the final lung region. Fig. 2 (e) shows the extracted binary mask of lung and it can be observed that the missing juxta-pleural nodules are added to the segmented lung. Finally, the extracted lung region is presented in Fig. 2 (f).

3.2 Candidate Nodule Detection

The effectiveness of an automated pulmonary lung nodule detection system depends on the accuracy of the detected nodule candidates. In the nodule candidate detection, initially ROIs are extracted based on the proposed optimal manifold statistical thresholding and then the nodule candidates are segmented from these ROIs.

The extraction of ROIs is complicated as the lung nodules have broader gray level range and varying level of vessel attachment. The optimal manifold statistical threshold is to overcome these complications. Earlier methods employed the mean or a fixed value as the base threshold in to multiple thresholding [16, 17], which may not always perform well. Therefore, we have calculated the new optimal statistical threshold value as a base threshold.

3.2.1 Optimal Statistical Thresholding Algorithm

a. Traditional Statistical Thresholding

Let the extracted lung region having L gray levels (0 to L-1) and the total number of pixels in the image is $N = n_0 + n_1 + ... + n_{L-1}$. The probability of i^{th} gray level is defined as

$$p_i = \frac{n_i}{N}, \quad p_i \geq 0, \qquad \sum_{i=0}^{L-1} p_i = 1, \tag{2}$$

That is, the number of pixels n_i having grey scale intensity 'i' as a fraction of the total number of pixels N .The lung region is separated into two classes C_B and C_O using a gray level 't'. Here, C_B is the background with levels '0' to 't', and the remaining pixels are the nodule candidates in C_O. Then the probabilities of these classes are defined as

$$n_B = \sum_{i=0}^{t} p_i \ , \tag{3}$$

$$n_O = \sum_{i=t+1}^{L-1} p_i \ , \tag{4}$$

The mean of the classes is defined as

$$\mu_B = \sum_{i=0}^{t} \frac{ip_i}{n_B}, \tag{5}$$

$$\mu_O = \sum_{i=t+1}^{L-1} \frac{ip_i}{n_O}, \tag{6}$$

The basic idea is to estimate μ_B - the average of the all corner pixels (background) and μ_O - the average of object pixels.

The variance of the classes is given by

$$\sigma_B^2 = \sum_{i=0}^{t} \frac{(i-\mu_B)^2 p_i}{n_B}, \tag{7}$$

$$\sigma_O^2 = \sum_{i=t+1}^{L-1} \frac{(i-\mu_O)^2 p_i}{n_O}, \tag{8}$$

Computing the intra-class variance, the inter-class variance and the total variance of the combined distribution is defined as

$$\sigma^2_{Within} = n_B\sigma^2_B + n_O\sigma^2_O, \tag{9}$$

$$\sigma^2_{Between} = n_B n_O(\mu_O - \mu_B)^2, \tag{10}$$

$$\sigma^2_{Total} = \sum_{i=0}^{L-1}(i-\mu_T)^2, \tag{11}$$

where $\mu_T = \sum_{i=0}^{L-1} ip_i$, According to the above equations, the following basic relation always holds:

$$\sigma^2_{Total} = \sigma^2_{Between} + \sigma^2_{Within}, \tag{12}$$

The variances intra and inter classes are functions of gray level 't' and the total class variance is independent of t. Minimization of intra-class variance is equivalent to Maximization of inter-class variance. Thus, the optimal threshold 't^*' can be determined by [23],

$$t^* = Arg^{\min}_{0\le t\le L-1}\left\{\sigma^2_{Within}\right\}, \tag{13}$$

The optimal threshold maximizes the inter-class variance of real-world images, but exhibits a limitation to classify an image into two parts of similar sizes regardless of the practical size of the object. After exploring the potential reason for the weakness, Hou's [24] developed a generalized version with a new threshold criterion, i.e., total class variance, and found the optimal threshold by minimizing it. The optimal threshold 't^*' can be defined as follows:

$$t^* = Arg^{\min}_{0\le t\le L-1}\left\{\sigma^2_{Total}\right\}, \tag{14}$$

b. Proposed New Criterion

The traditional methods only consider the sum of class variance, but neglect variance discrepancy between object and background of image. The typical example is in Fig. 4(a) where the nodule has slight gray level changes and small class variance, while the background has large gray level changes and large class variance. Its histogram of bimodal distribution with unequal sizes and groundtruth image are shown in Figs. 4(b) and (c). Manual threshold corresponding to the groundtruth image is 110, which locates it in between of two peaks. In this case those statistical thresholding methods find erroneous thresholds (i.e., 129 and 150) and fail to segment the object from background as shown in Fig. 4 (d) and (e). The reason is that the two approaches take only the sum of class variance into account, but neglect discrepancy of class variances. As an attempt to eliminate the limitations of these methods, a new statistical thresholding method is proposed in this paper.

The proposed method takes class variance sum and variance discrepancy into account at the same time and constructs an optimal statistical criterion for threshold selection, which can be formulated as

$$S(t) = \sigma^2_{Within}(t) + \alpha\sigma_{Discr}(t), \tag{15}$$

where $\alpha = |n_B - n_O|$, $\sigma_{Discr}(t) = \sigma_B(t)\sigma_O(t)$ and $\sigma^2_O(t) \le \sigma_{Discr}(t) \le \sigma^2_B(t)$ or $\sigma_{Discr}(t)\sigma^2_B(t) \le \sigma_{Discr}(t) \le \sigma^2_O(t)$ is used to measure variance discrepancy of two threshold classes. Here $\sigma_B(t)$ and $\sigma_O(t)$ are their respective standard deviations. The parameter α is a weight that balances the contributions of variance sum and variance discrepancy. When $\alpha = 0$ i.e $n_B = n_O$, the new criterion degenerates to Otsu's criterion

[23]. Thus the proposed method can be regarded as a generalized version of Otsu's method. An optimal threshold t^* can be found by minimizing the discrepancy in the new criterion

$$S(t^*) = Arg^{\min}_{0 \le t \le L-1} S(t), \tag{16}$$

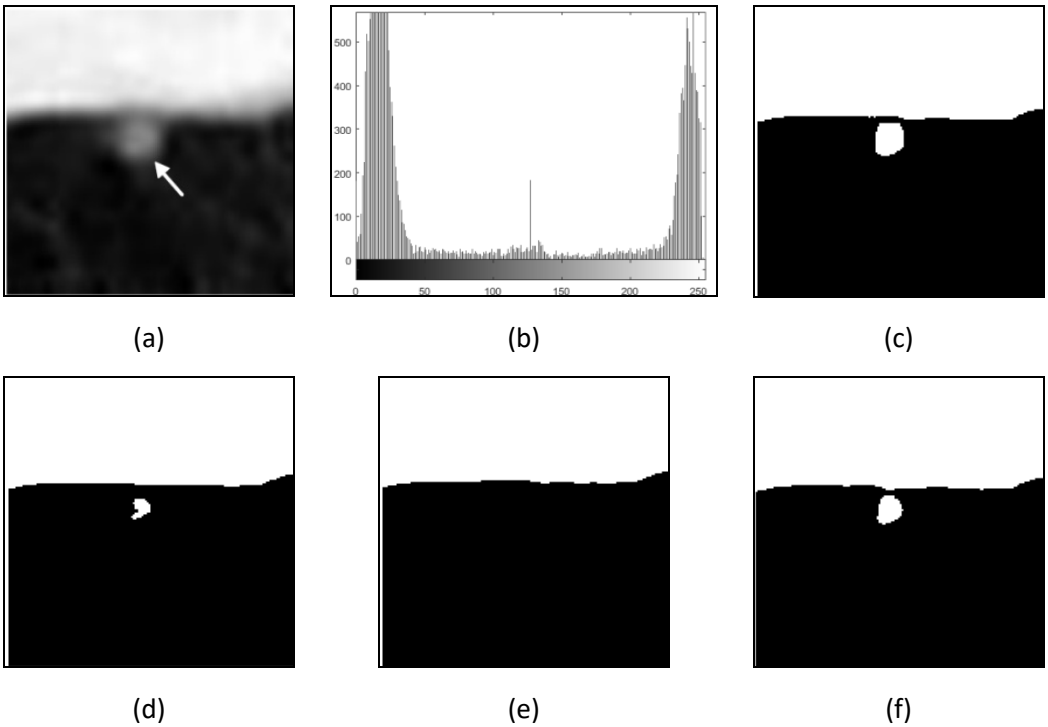

Figure. 4 Thresholding results of juxta-pleural nodule: (a) original, (b) histogram, (c) ground truth (t = 110), (d) Otsu's (t = 129), (e) Hou's (t= 150), (f) the proposed method (t =119)

Actually, equation (15) attempts to decrease the effect of class variance sum and emphasizes the influence of variance discrepancy simultaneously. In this way, the variance discrepancy becomes an explicit factor for determining the optimal threshold as shown in Fig. 4 (f).

3.2.2 Optimal Manifold Statistical Thresholds for ROI Extraction

The optimal statistical threshold t^* is the basic threshold for various nodule candidates and result of thresholding is shown in Fig. 4(f). The wide intensity range of nodules and the varying level of vessel attachment, make it difficult to extract ROIs. Optimal manifold statistical thresholds can be used to overcome these difficulties. To extract ROIs, we propose the use of optimal manifold statistical thresholding. Additionally six thresholds viz. $t^* - 200$, $t^* - 100$, $t^* + 100$, $t^* + 200$, $t^* + 300$, and $t^* + 400$ are used for the selection of ROIs. These ROIs are cumulative into one ROI image, i.e.

$$ROIs = \sum_{n=1}^{7} mask(I > t_n^*, S_i), \tag{17}$$

where I is the extracted lung region, t_n^* is the n^{th} optimal statistical threshold, and S_i is the segmented lung region mask. For the original chest CT image with groundtruth markings presented in Fig. 5 (a) and the ROIs are shown in Fig. 5 (b).

3.3 Classification of nodules and non-nodules

The resulting images shown in Fig. 5 (b) contain some blood vessels (non-nodules) along with the true nodules. We used SVM classifier to classify nodules and non-nodules based on the feature vectors extracted from the nodule candidates.

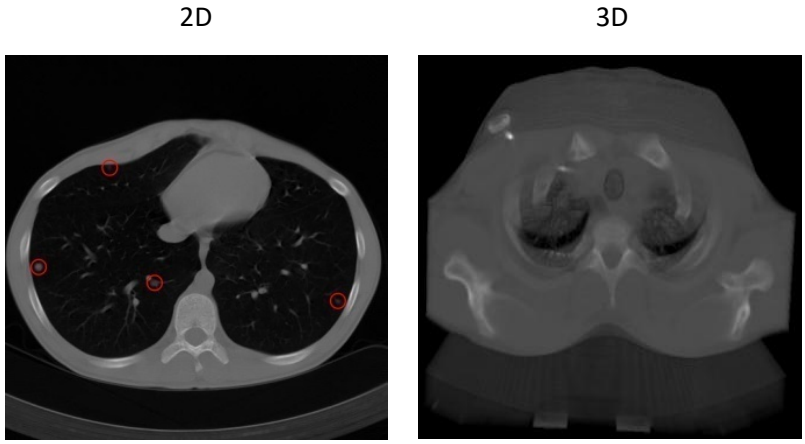

(a)

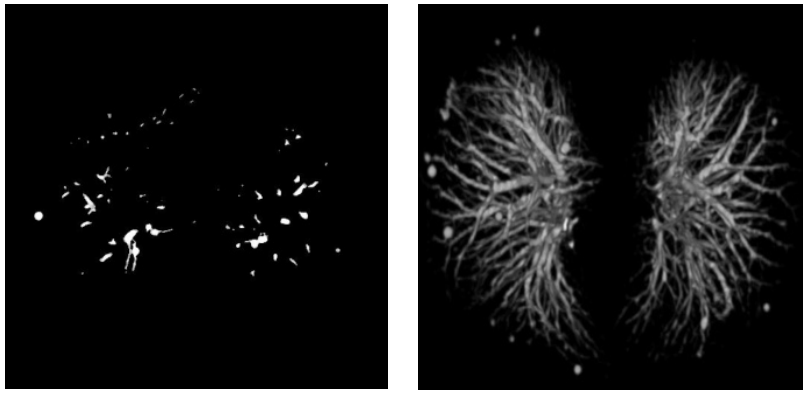

(b)

3.3.1 Feature Extraction

Here, we extracted ten features for training and classification, including six 2D features (area, diameter, circularity, elongation, compactness, and moment), and four 3D features (surface area, volume, sphericity, and centroid offset).

The 2-D geometric features are extracted in the following manner:

1. The area is obtained by using the equation:

$$Area = \sum_{o \in O_m} o, \tag{18}$$

Here, O_m is a middle slice of the segmented object o because the area of the segmented object at the median slice is the largest.

2. The diameter D is a maximum bounding box length of O_m

3. The Circularity reflects the similar degree of ROI region to a circle as follows:

$$Circularity = \frac{Area}{4\pi r^2}, \tag{19}$$

where r is the radius of the circumscribed circle and is equal to $D/2$.

4. Elongation is an asymmetry degree of an object and is obtained as follows:

$$Elongation = \frac{r_{\min}}{r_{\max}}, \tag{20}$$

where $r_{\min}$, $r_{\max}$ are the measurement from the centroid to the nearest and farthest points on the boundary.

5. Compactness is defined as

$$Compactness = \frac{R_{inside}}{R_{outside}}, \tag{21}$$

R_{inside}, and $R_{outside}$ are the radius of inscribed and circumscribed circle of ROI. If the value of compactness approximates to 1, ROI is closed and compact to a circle.

6. Moment of ROI is defined as

$$Moment = \sum_{i=0}^{P-1}\sum_{j=0}^{Q-1}\frac{\left(f(i,j)\right)^2}{1+|i-j|}, \tag{22}$$

$f(i,j)$ is normalized gray-value of pixels of ROI; P and Q are the number of rows and columns, respectively.

The 3-D geometric features are extracted in the following process:

7. Surface area of ROI as

$$A = \sum_{(x,y)\in S_i} P(x,y), \tag{23}$$

where $P(x,y)$ is the perimeter pixel number of ROI boundary, and S_i is the i^{th} slice of the ROI.

8. The volume of the segmented object is calculated as $V = N$. Here, N is sum of numbers of pixels whose gray scale is nonzero in all the ROI layers and it is defined as the volume of 3D ROI.
9. Sphericity is measure how much the shape of the object approximates to a spherical shape and is calculated as follows

$$Sphericity = \frac{6\sqrt{\pi}V}{A^{3/2}}, \tag{24}$$

10. Centroid offset is defined as

$$Center\ offset = \sum_{i=1}^{k}\left(|x_i-\bar{x}|+|y_i-\bar{y}|\right), \tag{25}$$

where k is number of ROI slices, (x_i, y_i) is the coordinate of centroid of the i^{th} slice, and (x,y) is the average coordinate of all the ROI slices.

3.3.2 SVM Classifier

SVM is very useful tool for object classification [10, 21, 25]. The basic SVM considers a set of input data and predicts two possible classes for each given input. Generally, the number of nodules is less than the number of non-nodules. This discrepancy affects the training of the classifier. Hence, we should balance the quantity of non-nodules and nodules. For this, we have randomly selected $N/2$ non-nodules and $N/2$ nodules from the obtained nodule candidates. The balanced dataset is then arbitrarily classified into testing and training datasets to validate the classifier. Suppose that we have a random sample of training dataset represented by $\left\{\left(X_i, y_i\right)\right\}_{i=1}^{N}$, $i=1,2,...,N$, where N is the number of training samples of nodule candidates, X_i in $\mathbb{R}^d$ is a feature vector, and y_i in $\{+1,-1\}$ indicates to linearly separable classes. The training data pair consists of an input feature vector and its equivalent known target class. The optimal solution of the SVM separating hyper-plane defined by a vector w in a high-dimensional space is

$$\min_{w,\xi} \frac{\lambda}{2}\left\|w^2\right\| + \sum_{i=0}^{N} \xi_i , \tag{26}$$

Therefore

$$f(X_i) = y_i \left\langle w, \Phi\left(X_i\right) \geq 1-\xi_i \right\rangle , \tag{27}$$

where $f(X_i)$ is the decision function, λ is a regularization parameter, $\xi_i \geq 0$ is slack variable, that indicates most of the cases are not linearly separable. In order to handle such cases, cost function need to be formulated for combining margin maximization and error minimization criteria. Φ is a non linear function that maps each data point into a higher dimensional space by a positive semi-definite kernel $k:\mathbb{R}^d \times \mathbb{R}^d \rightarrow \mathbb{R}$. This kernel is equivalent to an inner product in a higher dimensional space through $k\left(X, X^{'}\right) = \left\langle \Phi\left(X\right), \Phi\left(X^{'}\right) \right\rangle$.

Here, the radial basis function (RBF) is used as the kernel:

Radial basis function:

$$k_r\left(X_{i,} X_j\right) = \exp\left(\frac{-\left\|X - X_j\right\|^2}{p^2}\right) \tag{28}$$

where $p > 0$ is a kernels parameter.

The RBF kernel maps the feature space into a higher dimensional space to find an optimal segmentation hyper-plane. Nodules and non-nodules can be easily classified, once the classifier is trained. To obtain the nodule class from the test data, it requires an input feature vector of every nodule candidate. It is crucial to differentiate an input training and test datasets. In short, the lexicographical arrangement of input feature vectors is presented in a matrix $A = \left\{d^{(n)}\right\}_{n=1}^{N}$ of size $N \times M$, where d represents a

M dimensional feature vector, and N is the total number of feature vectors. The feature vector set is used to train the SVM for higher dimensional space to find an optimal segmenting hyper-plane.

In order to evaluate the SVM classifier, we have used k-fold cross validation. In k-fold cross validation, the original sample is subjectively divided into k sub-samples having equal size. Of the k sub-samples, a single sub-sample is selected as the validation data for testing the model and the remaining k - 1 sub-samples are used as training data. The cross validation process will be repeated for k folds with each of the k sub-samples. The results from the k folds are averaged to get a single estimation.

4 Results and Discussion

The performance of the proposed lung nodule detection system is evaluated using the publicly available Lung TIME database [22]. This database contains 148 CT scans. Each scan contains a varying number of image slices. On an average, 220 slices per scan are found and every slice has 512 × 512 pixels and 4K gray level values in HU, the resolution of image was 1.6 pixels per mm, slice spacing 1mm, slice thickness 5mm, and transversal resolution 0.58 ±0.06 mm. The database consists of 394 annotated nodules which covers almost every nodule type with 2-10 mm in diameter. Annotation is marked by two experienced radiologists. The database is in DICOM format and the data was acquired on Siemens CT machine.

Five performance measures viz. accuracy, sensitivity, specificity, geometric mean (G - mean) and F-measure are used to evaluate the proposed lung nodule detection system based on the following four possibilities:

- True positive (TP): the judgment by expert radiologists and the classifier prediction are both correctly labeled as object.
- False positive (FP): the judgment by experts is background, while the classifier prediction is object.
- True negative (TN): the judgment by experts and the classifier prediction are both background.
- False negative (FN): the judgment by experts is object, while the classifier prediction is background.

The accuracy is the fraction of all correctly classified pixels:

$$Accuracy = \frac{TP + TN}{TP + FP + TN + FN}, \tag{29}$$

When all pixels are correctly labeled, then accuracy is one.

The sensitivity is the fraction of correctly labeled object pixels:

$$Sensitivity(R) = \frac{TP}{TP + FN}, \tag{30}$$

A sensitivity of one indicates that all object pixels have been labeled correctly.

Specificity is the fraction of all correctly labeled background:

$$Specificity = \frac{TN}{FP + TN}, \tag{31}$$

For an unbalanced data classification performance evaluation criteria is geometric mean (G - mean), which is defined as

$$G\text{-}mean = \sqrt{Sensitivity * Specificity}, \tag{32}$$

G-mean maintains the balance between classification accuracies of the two classes.

For the evaluation of SVM, a function of *F-measure* is a way of evaluation of accuracy and sensitivity of the classification results for positive class. Here the accurate rate of classification of positive class is defined as

$$P = \frac{TP}{TP + FP}, \tag{33}$$

The evaluation function of F-measure can be defined as follows:

$$F\text{-}measure = \frac{2*P*R}{P + R}, \tag{34}$$

Obviously, the optimum of classification is that F-measure gets the maximum value 1.

4.1 Lung region segmentation

The results of the lung region extraction for various lung slices as shown in Fig. 6. The input thoracic CT images are shown in the first column. The second column presents corresponding lung region mask for the input CT images in first column. To generate the lung region mask, we set a threshold of -350 HU in order to separate the lung region from the thoracic CT scan. From the second column it can be observed that the extracted lung region is under segmented as the images we have considered have parenchymal lung diseases which include honeycombing, ground glass opacity, emphysema, and juxta-pleural nodules. The results of the proposed modified convex hull algorithm are given in the third column. The proposed method provides more accurate lung segmentation results as the algorithm uses the monotonicity property to extract the convex hull of an object such that the accuracy in segmentation and the computing speed increases.

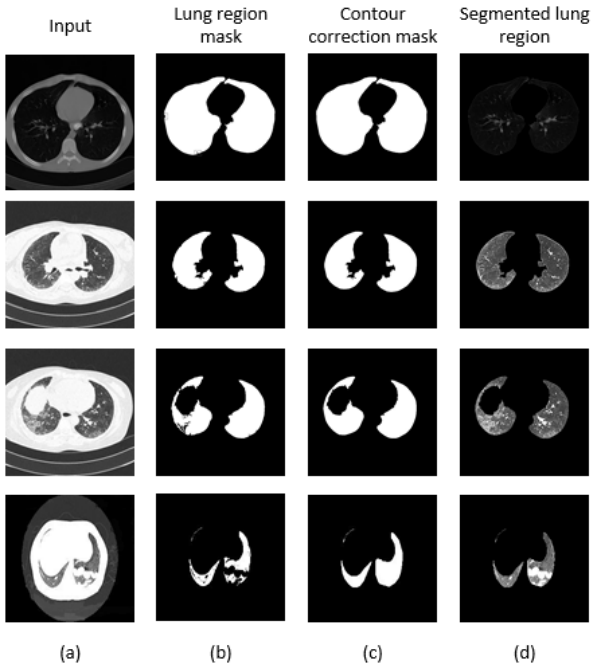

Figure.6 Results of lung region segmentation

The proposed algorithm has a very less computational cost in the following ways: (1) It divides the binary image into several regions by using the extreme points such that only those boundary pixels in few regions require computation. (2) The boundary pixels obtained by scanning are computed dynamically and only these vertices of temporary convex hull require storage. The segmented lung region is shown in the last column. Table 1 presents the results of proposed lung region segmentation algorithm before and after contour correction in terms of accuracy, sensitivity and specificity. The results yield comparable accuracies before and after contour correction. To enhance the sensitivity of this contour correction internal and sub-pleural lung regions are then truncated. The specificity indicates the probability of obtaining a negative result when the lung regions don't have the disease after contour correction.

Table 1 Summary of quantitative evaluation of lung region segmentation results before and after the contour correction by improved convexity algorithm. Numbers represent average ± standard deviation.

	Accuracy	Sensitivity	Specificity
Before	0.94 ± 0.06	0.90 ± 0.23	0.99 ± 0.01
After	0.95 ± 0.04	0.98 ± 0.14	0.96 ± 0.02

4.2 Nodule candidate detection

The proposed nodule candidate detection method is performed on the segmented lung regions. ROIs for the nodule candidates are extracted from the segmented lung region using optimal multiple statistical thresholding. Fig.7 presents the detected lung nodule candidates after applying optimal multiple statistical thresholding. The proposed method has detected 326 nodules with 31,743 FPs with a sensitivity of 94.29% and FPs of 214.4 per scan. In new optimal statistical thresholding, we have considered sum of the class variance and variance discrepancy of the object and background for threshold selection, the method obtained good results while segmenting small nodules which are isotropic or nearer to vessels and other structures.

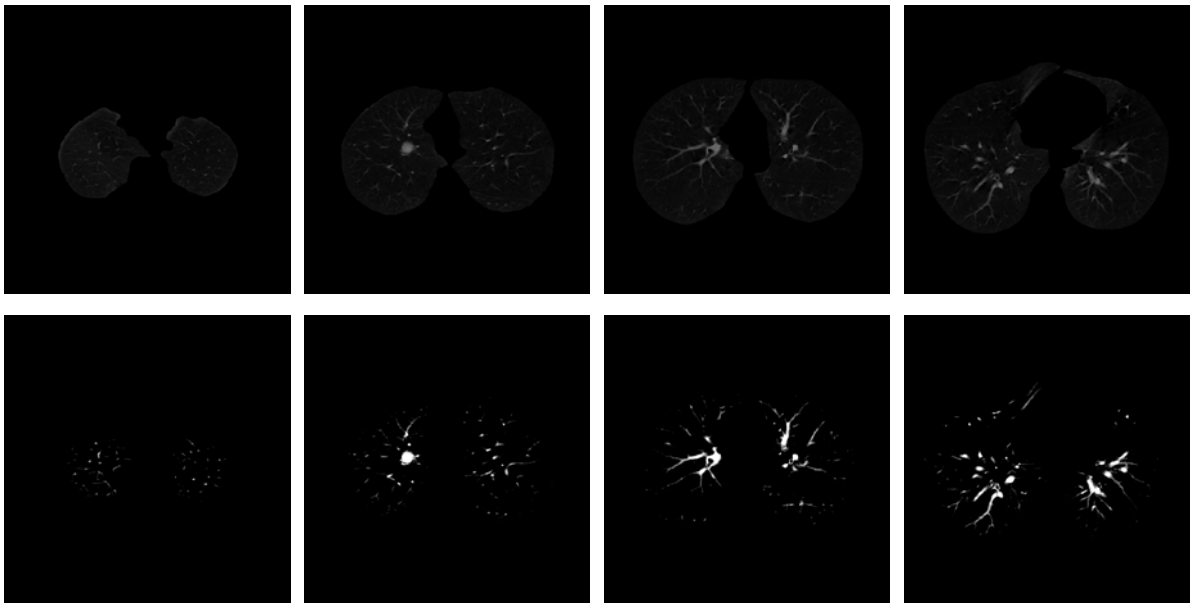

Figure. 7 The results of nodule candidate detection: extracted lung region(upper row), nodule candidate(bottom row) detection by proposed method

We have selected 326 non-nodules randomly from the detected non-nodule candidates and these non-nodules are then combined with 326 nodules to generate a balanced dataset for training. Finally, we have classified the detected nodule candidates into nodules and non-nodules using SVM classifier with radial basis function as kernel. The 2D and 3D orientations of the detected nodules and non-nodules by the SVM classifier are as shown in Fig. 8. In order to evaluate the SVM classifier, we have used k-fold cross validation. In this work, k =7 is used for evaluation as it provides a good balance between training and testing data for evaluating the proposed method than 5-fold and 10-fold cross validation. Table 2 shows the performance of SVMs for different k values.

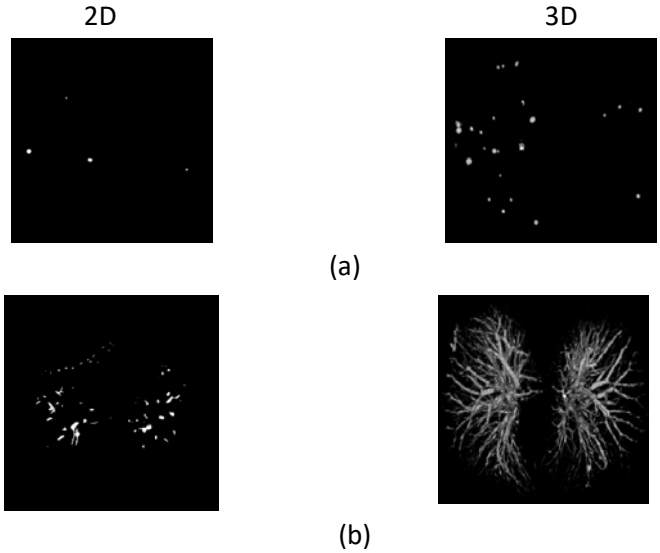

Figure. 8 The results of Fig. 5(b) nodule candidates: (a) nodule, (b) non-nodule

Table 2 The k-fold cross validation results of SVM classifiers with radial basis function kernel for different k values

k	Performance for data set (%)						
	Sensitivity	Specificity	Accuracy	PPC	G-Mean	F-measure	FPs/Scan
5	90.09	91.99	91.98	90.09	91.04	90.09	2.7
7	94.29	92.64	92.65	92.34	93.46	93.3	2.6
10	90.99	92.07	92.06	90.99	91.53	90.99	2.9

4.3 SVM classifier

The proposed classification approach achieved a sensitivity of 94.29%, specificity is 92.64%, accuracy is 92.65 %, G-mean 93.46% and an F-measure is 93.3% with 2.6 false positives per scan in the range of 2-10 mm in diameter of nodule size. All other CAD systems have reasonable sensitivity values in classification of pulmonary nodules. It is extremely important to consider the small nodule size in the classification of a CAD system. This increases the probability of early detection of nodules. Considering these results, it can be said that the proposed study represents a relatively high sensitivity. The Fig. 9 shows the ROC curve of the SVM classifiers.

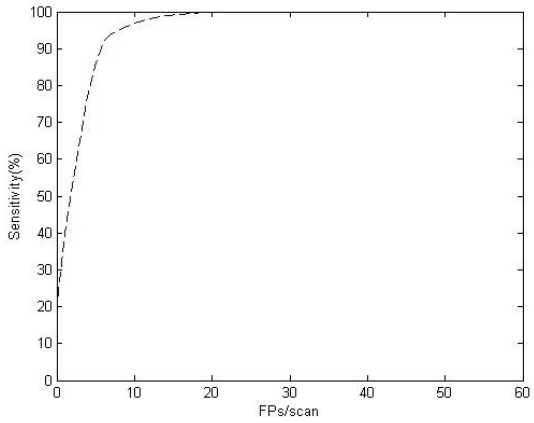

Figure. 9 Estimation of ROC curve for our algorithm.

We used recently reported lung nodule detection systems [7] [14] - [16], [18], [19] to compare and evaluate the results of proposed lung nodule detection system. The comparison with other lung nodule detection systems is difficult, as they used different database having different nodule orientations and sizes. The reported CAD systems used LIDC database in which the size of the nodules ranges from 3 mm to 30 mm. Table 3 presents the comparison of the proposed system with other systems. It can be observed from the table that the proposed system shows significantly better sensitivity with high reduced false positives. The system achieves 2.6 FPs per scan, with 93.3% sensitivity.

Table 3 Reported of performance comparison of CAD system

CAD systems	Number of cases	Number of nodules	Nodule size criterion used (mm)	Sensitivity (%)	Average FPs per case
Messay et al. [7]	84	143	3–30	82.66	3
Golosio et al. [14]	84	148	3–30	79	4
Dehmeshki et al. [15]	70	121	3–20	90	14.6
Pu et al [16]	22	71	≥3	76	3
Suzuki et al. [18]	71	121	8–20	80.3	16.1
Cascio et al. [19]	84	148	3–30	97.66	6.1
Proposed system	**148**	**355**	**2–10**	**94.3**	**2.6**

5 Conclusions

This paper presents an expert system to detect pulmonary nodules from chest CT scans using a feature descriptor based on optimal manifold statistical thresholding. The key features of the expert system are 1. A modified convex hull algorithm that is used to correct the lung contour which may be affected by dense abnormalities like juxta pleural nodules, ground glass obesity, etc and 2. A novel optimal manifold statistical thresholding algorithm can effectively detects the nodule candidates from segmented lung region. The modified convex hull algorithm uses the monotonicity property to extract the convex hull of an object such that the accuracy in lung region segmentation and the computing speed increases. The proposed optimal manifold statistical thresholding is used to segment the nodule candidates by considering the class variance sum and variance discrepancy simultaneously. The proposed method can be regarded as a generalized version of Otsu's method. The proposed system is evaluated on the publicly available Lung TIME database, and the results are compared with the results of recently reported systems. The proposed system shows the reduction of the false positive rate (2.6 FPs per scan) significantly while maintaining a high sensitivity of 94.3%. Hence, it is suitable for application in clinical lung cancer CAD systems.

REFERENCES

[1]. Siegel RL, Miller KD, Jemal A. Cancer statistics, 2015. CA: a cancer journal for clinicians. 2015 Jan 1;65(1):5-29.

[2]. Ballangan C, Wang X, Fulham M, Eberl S, Feng DD. Lung tumor segmentation in PET images using graph cuts. Computer methods and programs in biomedicine. 2013 Mar 31;109(3):260-8.

[3]. Thomsen LP, Weinreich UM, Karbing DS, Jensen VG, Vuust M, Frøkjær JB, Rees SE. Can computed tomography classifications of chronic obstructive pulmonary disease be identified using Bayesian networks and clinical data?. Computer methods and programs in biomedicine. 2013 Jun 30;110(3):361-8.

[4]. Samuel CC, Saravanan V, Devi MV. Lung nodule diagnosis from CT images using fuzzy logic. InConference on Computational Intelligence and Multimedia Applications, 2007. International Conference on 2007 Dec 13 (Vol. 3, pp. 159-163). IEEE.

[5]. Suárez-Cuenca JJ, Tahoces PG, Souto M, Lado MJ, Remy-Jardin M, Remy J, Vidal JJ. Application of the iris filter for automatic detection of pulmonary nodules on computed tomography images. Computers in Biology and Medicine. 2009 Oct 31;39(10):921-33.

[6]. Retico A, Delogu P, Fantacci ME, Gori I, Martinez AP. Lung nodule detection in low-dose and thin-slice computed tomography. Computers in biology and medicine. 2008 Apr 30;38(4):525-34.

[7]. Messay T, Hardie RC, Rogers SK. A new computationally efficient CAD system for pulmonary nodule detection in CT imagery. Medical image analysis. 2010 Jun 30;14(3):390-406.

[8]. Sluimer I, Prokop M, Van Ginneken B. Toward automated segmentation of the pathological lung in CT. IEEE transactions on medical imaging. 2005 Aug;24(8):1025-38.

[9]. van Rikxoort EM, de Hoop B, Viergever MA, Prokop M, van Ginneken B. Automatic lung segmentation from thoracic computed tomography scans using a hybrid approach with error detection. Medical physics. 2009 Jul 1;36(7):2934-47.

[10]. De Nunzio G, Tommasi E, Agrusti A, Cataldo R, De Mitri I, Favetta M, Maglio S, Massafra A, Quarta M, Torsello M, Zecca I. Automatic lung segmentation in CT images with accurate handling of the hilar region. Journal of digital imaging. 2011 Feb 1;24(1):11-27.

[11]. Paik DS, Beaulieu CF, Rubin GD, Acar B, Jeffrey RB, Yee J, Dey J, Napel S. Surface normal overlap: a computer-aided detection algorithm with application to colonic polyps and lung nodules in helical CT. IEEE transactions on medical imaging. 2004 Jun;23(6):661-75.

[12]. Armato SG, Giger ML, Moran CJ, Blackburn JT, Doi K, MacMahon H. Computerized detection of pulmonary nodules on CT scans 1. Radiographics. 1999 Sep;19(5):1303-11.

[13]. Pulagam AR, Kande GB, Ede VK, Inampudi RB. Automated Lung Segmentation from HRCT Scans with Diffuse Parenchymal Lung Diseases. Journal of digital imaging. 2016 Aug 1;29(4):507-19.

[14]. Golosio B, Masala GL, Piccioli A, Oliva P, Carpinelli M, Cataldo R, Cerello P, De Carlo F, Falaschi F, Fantacci ME, Gargano G. A novel multithreshold method for nodule detection in lung CT. Medical physics. 2009 Aug 1;36(8):3607-18.

[15]. Dehmeshki J, Ye X, Lin X, Valdivieso M, Amin H. Automated detection of lung nodules in CT images using shape-based genetic algorithm. Computerized Medical Imaging and Graphics. 2007 Sep 30;31(6):408-17.

[16]. Pu J, Paik DS, Meng X, Roos J, Rubin GD. Shape “break-and-repair” strategy and its application to automated medical image segmentation. IEEE transactions on visualization and computer graphics. 2011 Jan;17(1):115-24.

[17]. Osman O, Ozekes S, Ucan ON. Lung nodule diagnosis using 3D template matching. Computers in Biology and Medicine. 2007 Aug 31;37(8):1167-72.

[18]. Suzuki K, Armato SG, Li F, Sone S. Massive training artificial neural network (MTANN) for reduction of false positives in computerized detection of lung nodules in low-dose computed tomography. Medical physics. 2003 Jul 1;30(7):1602-17.

[19]. Cascio D, Magro R, Fauci F, Iacomi M, Raso G. Automatic detection of lung nodules in CT datasets based on stable 3D mass–spring models. Computers in Biology and Medicine. 2012 Nov 30;42(11):1098-109.

[20]. Choi WJ, Choi TS. Automated pulmonary nodule detection based on three-dimensional shape-based feature descriptor. Computer methods and programs in biomedicine. 2014 Jan 31;113(1):37-54.

[21]. da Silva Sousa JR, Silva AC, de Paiva AC, Nunes RA. Methodology for automatic detection of lung nodules in computerized tomography images. Computer methods and programs in biomedicine. 2010 Apr 30;98(1):1-4.

[22]. Dolejší M, Kybic J. Automatic two-step detection of pulmonary nodules. InMedical Imaging 2007 Mar 8 (pp. 65143J-65143J). International Society for Optics and Photonics.

[23]. Otsu N. A threshold selection method from gray-level histograms. Automatica. 1975 Jun;11(285-296):23-7.

[24]. Hou Z, Hu Q, Nowinski WL. On minimum variance thresholding. Pattern Recognition Letters. 2006 Oct 15;27(14):1732-43.

[25]. Osuna E, Freund R, Girosi F. Support vector machines: Training and applications. 1997.

